nature photonics

ARTICLES

PUBLISHED ONLINE: 24 OCTOBER 2010 | DOI: 10.1038/NPHOTON.2010.235

Real-space imaging of transient carrier dynamics by nanoscale pump–probe microscopy

Yasuhiko Terada, Shoji Yoshida, Osamu Takeuchi and Hidemi Shigekawa*

Smaller and faster are key concepts underlying the progress of current nanoscience and nanotechnology. The development of a method of exploring the transient carrier dynamics in organized nanostructures with pinpoint accuracy is therefore highly desirable. Here, we present a new microscopy that enables real-space measurement of the spatial variation of ultrafast dynamics. It is a pulse-laser-combined scanning tunnelling microscopy with a novel delay-time modulation method based on a pulse-picking technique. A non-equilibrium carrier distribution is generated with ultrashort laser pulses, and its relaxation processes are observed by scanning tunnelling microscopy using a pump–probe technique. We have directly analysed the recombination of excited carriers via the gap states associated with a cobalt nanoparticle/GaAs structure in real space. Through the site dependence of the decay time on the tunnelling current injection from the scanning tunnelling microscopy tip, the hole capture rate at the gap states has been imaged on the nanoscale for the first time.

The understanding and control of quantum dynamics, such as carrier transitions and transport in nanoscale structures, are key factors for continuing the advancement of nanoscale science and technology. However, with the miniaturization of functional devices consisting of composite materials, carrier dynamics, which has been analysed by techniques providing spatially and/or temporally averaged information, does not provide a sufficient description for the analysis and design of macroscopic functions. For example, atomic-scale defects have significantly changed the entire approach. Defects, which were once considered a problem to be avoided, are now actively designed and controlled to realize desired functions[1]. Fluctuation in the distribution of dopant materials in nanostructural components governs the characteristic properties of the macroscopic functions of the total system. Therefore, evaluation of the transient carrier dynamics on the nanoscale is of great importance.

The recent development of ultrashort-pulse laser technology has enabled the observation of ultrafast dynamics in the femtosecond range. A prominent method used for this is optical pump–probe reflectivity (OPPR) measurement[2,3]. Its spatial resolution, however, is generally limited by wavelength, and information is inevitably averaged over the nanoscale components, despite their careful organization to produce desired functions. In contrast, the real-space observation of atomic-scale structures by scanning tunnelling microscopy (STM) has addressed various longstanding problems and is extending the frontiers of science and technology[4–9]. However, because the temporal resolution of STM is limited to less than 100 kHz because of the circuit bandwidth, the target carrier dynamics has been beyond its field of vision. Since the invention of STM, one of the most challenging goals has been to combine it with ultrashort-pulse laser technology.

In their pioneering work, Hamers and colleagues determined the recombination lifetime of photoexcited carriers in silicon by analysing the observed surface photovoltage (SPV) by simulation[10]. Other methods that involve the combined use of an optical pulse pair and STM have also been proposed[11–18]. However, the spatial and temporal resolutions of the former method were limited to the 1 μm scale and the laser-pulse repetition rate, respectively, and the latter methods probe, for example, spatial variation in dI/dV rather than the transient dynamics itself[18]. With shaken-pulse-pair-excited STM (SPPX-STM)[19,20], which was designed to detect the weak tunnelling current of a transient signal under optical excitation, the time-resolved tunnelling current in the subpicosecond range was successfully probed. However, its temporal range was very narrow and it is still difficult to reliably measure a very weak time-resolved STM signal in a short period of time, preventing SPPX-STM from revealing transient carrier dynamics in nanostructures consisting of composite materials with a wide variety of lifetimes, as the long measurement time interferes with the imaging of dynamics.

Here, we demonstrate a new methodology, that simultaneously realizes STM spatial resolution together with the temporal resolution of the optical pump–probe technique, enabling the visualization of transient carrier dynamics in nanometre-scale structures with a wide variety of lifetimes. As an example, through the site dependence of the decay time on the tunnelling current injection from the STM tip, the first direct analysis of the hole capture rate via a gap state in a cobalt nanoparticle/GaAs structure is shown. Pinpoint probing and real-space imaging of a meaningful physical quantity in nanometre-scale structures have been realized.

Results

Nanoscale pump–probe microscopy and its fundamentals. Figure 1 shows a schematic of the microscopy technique and its basic probing mechanism. The surface of a sample beneath an STM tip is illuminated with a sequence of paired laser pulses with a certain delay time t_d, and the (temporally averaged) tunnelling current I is measured as a function of t_d (Fig. 1a). The optical pulses create an excited state in the sample, resulting in a rapid change in a physical quantity n such as the photocarrier density in a semiconductor (Fig. 1c), which often gives rise to changes in the raw tunnelling current I^* (Fig. 1d), reflecting the excitation and relaxation of the sample. When t_d is sufficiently long, paired optical pulses with the same intensity independently induce two excitation pulses with the same height in n (Fig. 1c,i). In contrast, when t_d is short and the second pulse illuminates the sample in an excited state caused by the first optical pulse, the second excitation in n may have a different intensity, depending on t_d

Institute of Applied Physics, CREST-JST, University of Tsukuba, Tsukuba 307-8573, Japan. *e-mail: hidemi@ims.tsukuba.ac.jp

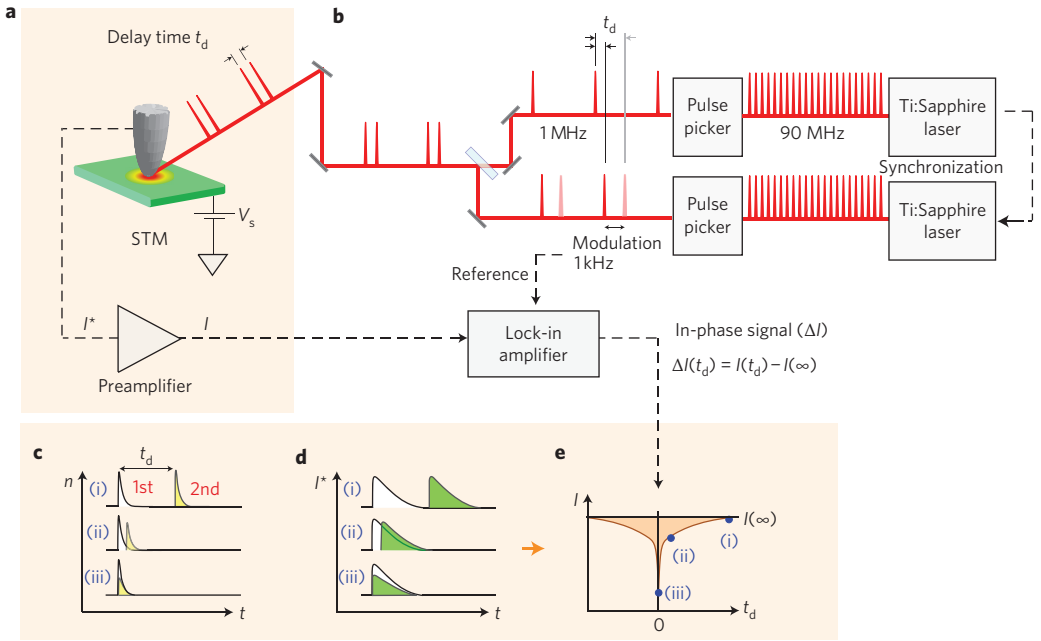

Figure 1 | Schematics of the microscopy system and its probe mechanism. a,**b**, Optical pulses from the two synchronized lasers are selectively transmitted using pulse pickers and coaxially aligned to produce a sequence of paired pulses with a certain delay time t_d. Pulse pairs were focused to less than 10 μm, and the tunnelling current was measured. **c**, Relationship between photoexcitation and delay time t_d. **d**, Change in transient tunnelling current induced by the excitation in **c**. **e**, Measured tunnelling current $I(t_d)$, where delay times in (i), (ii) and (iii) correspond to those in (i), (ii) and (iii) in **c** and **d**.

(Fig. 1c,ii,iii). Although the lifetime of the excited state is, in general, different from the decay time of I^*, the change in n strongly affects the second pulse in I^*. Thus, the change in I^*, and thereby the signal I, also depends on t_d, because the height difference in the second current pulse in I^* changes the temporally averaged value of the tunnelling current (Fig. 1e). Accordingly, the relaxation dynamics of the excited state in the target material, namely the change in a physical quantity after excitation by the first optical pulse, can be probed by STM at the pulse-width resolution (that is, in the femtosecond range). In principle, we can obtain the temporal resolution of OPPR together with the spatial resolution of STM.

To realize the desired microscopy, we developed a method for the large and discrete modulation of delay time using a pulse-picking technique (Fig. 1b, see Methods). With the digital modulation of t_d between t_d^1 and t_d^2, the in-phase component obtained by lock-in detection of the tunnelling current gives $\Delta I(t_d^1,t_d^2) \equiv I(t_d^1) - I(t_d^2)$. As t_d^2 is set to a value larger than the relaxation time of the probed dynamics, $\Delta I(t_d^1,t_d^2)$ can be approximated as $\Delta I(t_d^1) \equiv I(t_d^1) - I(\infty)$, where $I(\infty)$ is the tunnelling current for a delay time that is sufficiently long for the excited state to be relaxed. Because a large delay time to satisfy this condition ($t_d^2 = \infty$) can be realized with the new microscopic technique, $\Delta I(t_d^1)$ is accurately obtained through the lock-in detection of I by sweeping t_d^1. In addition, because the modulation can be performed at a high frequency (1 kHz in our case), the measurement is hardly affected by low-frequency fluctuations in the laser intensity and tunnelling current. Accordingly, this method improves the signal-to-noise ratio (SNR) by a factor of 100 for our system compared with the method of mechanical modulation using mirrors, and therefore enables the spatial mapping of time-resolved signals, which has long been desirable.

SPPX signal from semiconductor. Figure 2 presents sample spectra obtained using this microscopic technique. For the first time, the measurement of carrier dynamics over a wide range of timescales has been achieved using a single microscope. A low-temperature-grown GaAs (LT-GaAs) region formed on a GaAs substrate

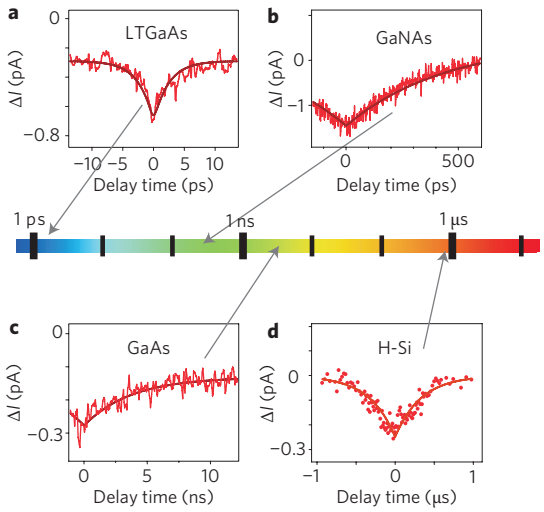

Figure 2 | Carrier dynamics over a wide range of timescales measured using the developed microscopy. a–**d**, $\Delta I(t_d)$ versus t_d curves obtained for LT-GaAs (**a**), GaNAs (**b**), undoped GaAs (**c**) and hydrogen-terminated Si(111) (n-type, 0.5 Ω cm) (**d**). The decay constants derived by fitting are 2.4 ps (**a**), 440 ps (**b**), 4.8 ns (**c**) and 0.87 μs (**d**). See 'Fitting Procedures' in Supplementary Information for more details.

exhibits an ultrafast decay component τ_b with a time constant of 2.4 ps, and the GaAs substrate region exhibits a time constant of 4.8 ns. These values are consistent with the recombination lifetimes determined from OPPR measurements, namely 1.5 ps and 3.3 ns for the LT-GaAs and GaAs samples, respectively. Such agreement has been confirmed for various semiconductors with a wide range of lifetimes (Supplementary Fig. S1).

When the delay time is changed over a wider range of timescales, $\Delta I(t_d)$ exhibits a slower component with a time constant of ~100 ns for both the GaAs and LT-GaAs regions, as shown in the typical

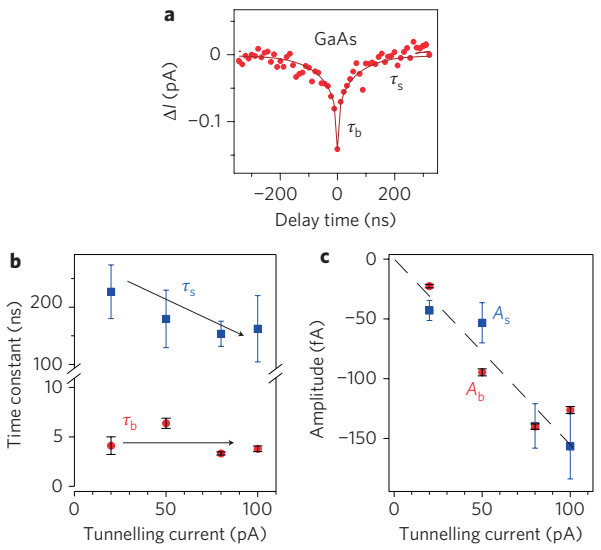

Figure 3 | Bulk-side and surface-side carrier decay reflected in $\Delta I(t_d)$. **a**, Typical spectrum obtained for GaAs over a wider range of timescales ($V_s = 5.5$ V, $I_t = 40$ pA). The components with small and large time constants τ_b and τ_s represent bulk-side and surface-side decay, respectively. **b**,**c**, Dependence of the decay constants on set-point tunnelling current I_t ($V_s = 5$ V).

spectrum obtained for GaAs in Fig. 3a. Although the decay process for a semiconductor is complex, a possible mechanism can be described as follows (see 'Mechanism' in Supplementary Information). In STM of a semiconductor, a nanoscale metal–insulator–semiconductor (MIS) junction is formed by the STM tip, tunnelling gap and sample. Thus, when a reverse bias voltage is applied to the junction, tip-induced band bending (TIBB) occurs in the surface region owing to leakage of the electric field into the sample[9,18,21]. Upon optical illumination, the redistribution of photocarriers reduces the electric field and changes the surface potential (SPV), thus increasing the effective bias voltage applied to the tunnel junction. Consequently, the illumination increases the raw tunnelling current I^*. The excited state subsequently relaxes to the original state through two processes. One is the decay of photocarriers on the bulk side (bulk-side decay) by means of recombination, drift and diffusion. The other is the decay of carriers trapped at the surface (surface-side decay) through recombination and thermionic emission. Because of the lack of counterpart carriers near the surface, the surface-side decay constant is larger than the bulk-side decay constant.

The bulk-side decay is probed through the mechanism of absorption bleaching, which is a typical mechanism observed in OPPR measurement. The carriers excited by the first optical pulse remain in the excited state, but the absorption of the second optical pulse is suppressed. The total number of carriers excited by the two optical pulses changes with t_d, resulting in the total tunnelling current depending on t_d. On the other hand, the surface-side decay is probed through the mechanism related to SPV. If surface carriers remain when the second optical pulse arrives, the electric field in the surface region remains low. Therefore, the excited photocarriers are less efficiently trapped at the surface, leading to a decrease in SPV caused by the second optical pulse, and therefore a reduction in the height of the second current pulse in I^*. Accordingly, $\Delta I(t_d)$ is a measure of surface-side carrier density at the delay time t_d, as well as bulk-side carrier density.

The decay constants for both components are derived from the fitting of $\Delta I(t_d)$ by a double exponential function; the small time constant τ_b is attributed to bulk-side decay (Fig. 2 and Supplementary Fig. S1), and the large time constant τ_s to surface-side decay (Fig. 3a). We next show the results obtained for a cobalt/GaAs system. This is the first demonstration that a meaningful physical quantity can be directly derived from the analysis of τ_s on the nanoscale, which also provides more specific evidence for our mechanism.

Real-space probing of gap-state-enhanced carrier recombination. If a gap state exists in a bandgap, minority carriers are captured at the gap state with a high probability, and then rapidly recombine with majority carriers. The modulation of carrier dynamics due to gap states significantly affects the properties of a device, and therefore a new method that enables the direct analysis of gap-state-related processes at the nanoscale is strongly desired. As an example, we demonstrate the direct analysis of the hole capture rate through a cobalt-derived gap state.

Figure 4a shows an STM image of cobalt nanoparticles on an n-type GaAs surface. Cobalt particles grow in the Volmer–Weber mode[22] on GaAs, and their size is controllable. Nanoparticles are typically 2 nm in size (~400 atoms), which is sufficiently large to form a gap-state level[23,24].

Figure 4b,c shows $\Delta I(t_d)$ curves measured at positions corresponding to bare GaAs and cobalt, respectively. The peak ratio of the bulk-side decay component to the surface-side decay component varies with the excitation intensity; the bulk-side decay decreases as the excitation intensity increases. Here, we adjusted the excitation intensity to observe only surface-side decay. As expected, the decay constant at cobalt, 42 ns, is shorter than that at the bare GaAs surface, 223 ns.

A depletion layer is formed beneath the tip because of TIBB (Fig. 4d) as well as the band bending induced by the gap states in the present case. The holes (minority carriers) photogenerated in the depletion layer drift to the surface and are rapidly captured at the gap states. However, the electrons (majority carriers) are depleted near the surface, and therefore no counterpart carriers exist that recombine with the holes captured at the gap states. The carrier decay time is nevertheless much shorter at the cobalt because the electrons are injected from the STM tip to the cobalt site by means of tunnelling.

This is confirmed by the dependence of carrier decay time at cobalt on tunnelling current (Fig. 4e). The decay time markedly decreases as tunnelling current increases. In addition, the decay time is almost constant ($T_{cap} = 6.9$ ns) above a threshold current I_c (120 pA). From the analysis below, the hole capture probability P_h was derived as $P_h = 1/T_{cap} = 1.5 \times 10^8$ (s^{-1}).

The hole capture rate J_h is written as $J_h = P_h N_h$, where P_h is the probability per second that a hole in the depletion layer is captured at a gap state, and N_h is the number of holes trapped at the surface after photoexcitation. The recombination process is governed by the tunnelling current directly injected into the gap state localized at the cobalt site. The rate of injection electrons to a gap state J_e is proportional to the tunnelling current I_t: $J_e = I_t/e$. Assuming that the rate of carrier recombination at the gap state is high[25], the recombination rate is equal to the lower of J_h and J_e. Thus, the recombination rate is J_e-limited when I_t is low, but is J_h-limited and independent of I_t when I_t is high. In the J_h-limited regime, J_h varies with N_h, and the time evolution of N_h is written as

$$\frac{dN_h}{dt} = -J_h = -P_h N_h, \quad N_h = N_{h0} \exp(-P_h t)$$

Here, the hole decay rate is equal to P_h.

For $I_c < I_t$ (J_h-limited regime), the gap state is filled with tunnelling electrons, and even if N_h is large immediately after photoexcitation, $J_h < J_e$ and the recombination rate is P_h, independent of I_t. Accordingly, the hole capture rate P_h can be directly derived from the decay time in this regime.

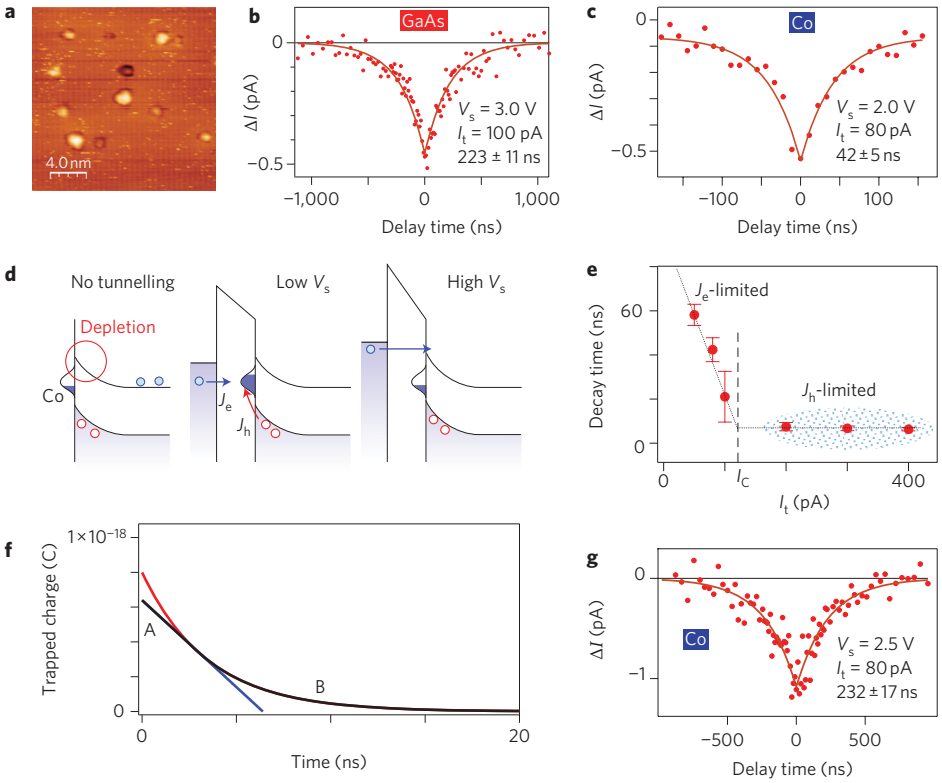

Figure 4 | Carrier recombination via cobalt nanoparticle/GaAs gap states. a, STM image of cobalt nanoparticles on a GaAs(110) surface. **b**,**c**, SPPX signals measured above bare GaAs and a cobalt nanoparticle. **d**, Schematics of surface-side recombination. **e**, Tunnelling current dependence of carrier decay time at cobalt ($V_s = 2$ V). **f**, Simulation of the SPPX signal with two decay modes when $I_t < I_c$. **g**, SPPX-STM signal at a high bias voltage.

For $I_t < I_c$, on the other hand, N_h is large and $J_h > J_e$ immediately after photoexcitation, and N_h initially decays linearly with time (A in Fig. 4f). Subsequently, when N_h becomes small and $J_h < J_e$, N_h starts to decay exponentially (B in Fig. 4f). The time evolution of N_h is therefore represented as a black line in Fig. 4f. Because the SNR was not sufficient to distinguish between linear and exponential decay, the fit to the data was carried out with a single exponential function. Therefore, the apparent decay time derived from the fitting should be larger than P_h^{-1}, which was indeed observed as shown in Fig. 4e.

When $I_t = I_c$, J_e is equal to J_h at the excitation time; this relation gives the number of holes N_{h0} photogenerated in the depletion layer and trapped beneath the tip. From Fig. 4e, $I_c =$ 120 pA ($J_e = 7.5 \times 10^8$ s^{-1}) and N_{h0} is derived to be 5.0. This value is comparable to the number of charges N_0 estimated to exist between a sphere of radius R and an infinite plane placed at a distance of 1 nm from the sample; N_0 is 15.5 for $R = 10$ nm and 40.7 for $R = 20$ nm.

Next we show probing of hole capture rate in real space (Fig. 5). The decay time is short directly above a cobalt nanoparticle and markedly increases when the tip is placed at a subnanometre distance away from it. This feature is consistent with the fact that the recombination is markedly accelerated only when tunnelling electrons are injected from the STM tip to the gap states formed by the cobalt nanoparticle.

Furthermore, the result shown in Fig. 5 confirms that the hole capture rate for each cobalt nanoparticle is distinguishable when the nanoparticles are at least 1 nm apart. Accordingly, we measured T_{cap} for cobalt nanoparticles with different sizes (Fig. 5d). As the cobalt base area (S) increases, the capture probability is expected to increase and thus T_{cap} decreases, which corresponds well to the obtained result shown in Fig. 5d.

Thus, the new microscopy method enables the measurement of the carrier capture rate at a surface in real space. The solid line in Fig. 5d is the fit to the data with the simplified function $T_{cap} \approx 1/S$ (ref. 26). The discrepancy in the fitting is considered to be due to the use of a simplified model.

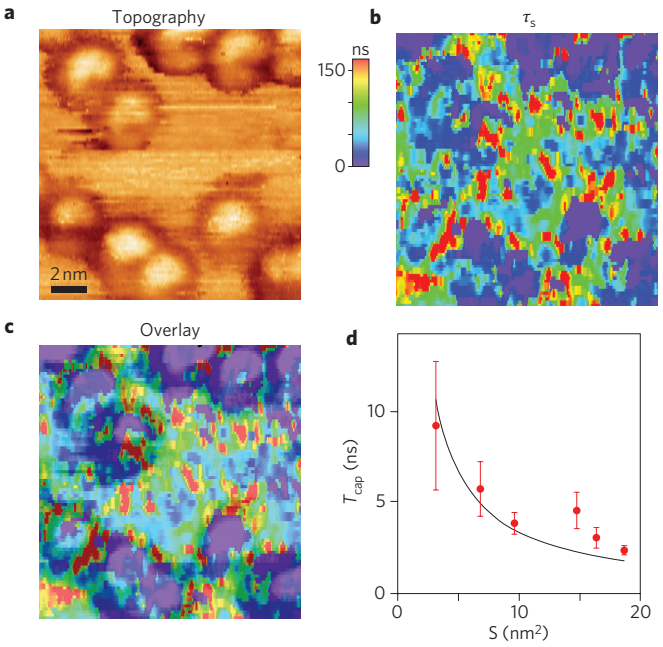

Figure 5 | Real-space analysis of the hole capture rate at cobalt nanoparticle/GaAs gap states. a,**b**, STM image (**a**) and two-dimensional mapping of time-resolved signal (**b**) obtained for a cobalt nanoparticle/GaAs(110) system. **c**, Image of **a** superimposed on **b. d**, Size dependence of hole capture rate.

Discussion

Here, we discuss the processes occurring in SPPX-STM measurement in more detail. The faster of the two decay components appearing in $\Delta I(t_d)$ is considered to reflect the decay of bulk-side carriers, which are probed on the basis of absorption bleaching. This is well supported by the fact that τ_b is consistent with the decay time obtained by the OPPR measurement of various samples (Supplementary Fig. S1). On the other hand, the slower decay component τ_s has a complex dependence on tunnelling current and sample bias voltage, which is consistent with the characteristic of surface-side carrier decay.

Because recombination at the surface is enhanced for a large set-point tunnelling current I_t, τ_s decreases as I_t increases. In contrast, the bulk-side carrier decay is not affected by the magnitude of I_t. Therefore, τ_b is independent of I_t. These expectations were confirmed, as shown in Fig. 3b; τ_s decreases with I_t, while τ_b remains almost constant. The linear relationship between signal amplitude and set-point tunnelling current (Fig. 3c) indicates that the time-resolved signal does not originate, for example, from photoelectrons and the displacement current, but from the tunnelling current (see 'Mechanism' in Supplementary Information).

The mechanism for the cobalt nanoparticle/GaAs is confirmed by its dependence on the sample bias voltage V_s. For high V_s, the Fermi level of the tip is higher than the conduction band minimum of the sample. Because the tunnelling probability for an electron is higher when its energy is closer to the vacuum level, electrons directly tunnel to the conduction band (Fig. 4d). In this case, accelerated recombination via the gap state is less probable. This expectation was experimentally confirmed. For $V_s = 2.5$ V (Fig. 4g), the surface-side decay constant was 232 ns, comparable to that for the bare GaAs (Fig. 4b).

As the device size decreases, the nanoscale modification of carrier dynamics, for example by atomic-scale defects, will strongly affect the macroscopic device properties, so an urgent task is to understand and control the correlation between structural fluctuations and carrier dynamics. The microscopic process of intrinsic, surface and bulk carrier dynamics is complex, particularly in an inhomogeneous sample. Although further analysis is required, it is of great significance that our new microscopic technique provides data that can be used to discuss the dynamics in nanosystems.

By combining advanced ultrashort-pulse laser technology with STM, we have developed a new microscopy technique that achieves the spatiotemporal imaging of ultrafast dynamics. The time resolution of this microscopy is limited only by the optical pulsewidth, which is 140 fs in the present case (see 'Fitting Procedures and Time Resolution' in Supplementary Information). As a demonstration of this microscopy technique, real-space probing of gap-state-enhanced carrier recombination for a cobalt nanoparticle/GaAs structure has been shown. Through the site-dependence of the decay time on the tunnelling current injection from the STM tip, the hole capture rate at the gap states associated with a cobalt nanoparticle/GaAs structure has been imaged on the nanoscale for the first time.

SPPX-STM is also applicable to the systems in which the response of the tunnelling current has a nonlinear dependence on optical intensity. With the use of selected-wavelength and circularly polarized illumination, quantum transitions including excited and/or spin states may be probed. The direct observation of such dynamics is expected to enable further advances in nanoscale science and technology.

Methods

As shown in Fig. 1b, pulse trains were generated by two synchronized Ti:Sapphire lasers (Mira and Chameleon, Coherent Inc.; central wavelength, 800 nm; average intensity, 1 W) at a repetition rate of 90 MHz with a pulse width of 140 fs. The delay time between the two pulse trains could be continuously varied from zero to the pulse interval (~11 ns) by the synchronizing circuit (Synchrolock, Coherent Inc.), which had a time jitter of 600 fs. Each train was guided to a pulse picker, which consisted of an ultrafast Pockels cell and polarizers, and was controlled by a laboratory-built timing generator. The pulse picker selectively transmitted one pulse out of typically every 90 pulses, resulting in a pulse train with a reduced repetition rate of f_p (typically 1 MHz), while reducing the intensity of other pulses by a factor of 300. When the lifetime to be measured was longer than 0.5 μs ($=1/(2f_p)$), f_p was set to lower than 1 MHz to optimize the measurement in accordance with the lifetime. By changing the relative timing of pulse picking, an additional longer delay time was generated, which could be controlled to multiples of the original pulse interval (~11 ns). Combining the short delay time generated by the synchronizing circuit and the longer delay time generated by the pulse pickers, the total delay time could be adjusted continuously from zero to as large a value as required. Note that the reduced repetition rate could be set as low as required, reducing the average laser intensity. The two pulse trains were arranged onto the same light axis and guided into the STM (VT-STM, Omicron NanoTechnology GmbH). The light spot, which had a diameter of <10 μm and an average intensity of up to several milliwatts, was focused on a sample surface below the STM tip using two lenses placed outside the ultrahigh vacuum chamber (base pressure, $<1 \times 10^{-8}$ Pa). The light spot was precisely positioned to maximize the SPV effect appearing in the tunnelling current. All experiments discussed in this paper were carried out at room temperature.

Delay-time modulation was achieved by changing the pulse-picking timing periodically at a frequency of ~1 kHz. In the anterior half of the period, pulse picking was carried out at almost the same time for the pump and probe pulse trains, and in the posterior half of the period it was carried out with a difference of 180°. As a result, the delay time was modulated in a rectangular form between a relatively small value t_d (1 ps–1 μs) and a very large value (0.5 μs to several microseconds), by which the ultrafast phenomena completely reached the steady state. Synchronously with the delay-time modulation, the tunnelling current signal from the STM preamplifier with a bandwidth of ~10 kHz was phase-sensitively detected by a lock-in amplifier. By virtue of the rectangular modulation of the delay time, the output of the lock-in amplifier was proportional to the difference between the tunnelling current at the two delay times. In particular, when the larger delay time was set to be sufficiently long for the transient phenomena to reach the steady state, the signal became proportional to $\Delta I = I(t_d) - I(\infty)$. This novel technique of using pulse pickers to modulate the delay time in a rectangular form with a large amplitude and a high modulation frequency is essential for maximizing the SNR to achieve nanometre spatial resolution simultaneously with subpicosecond time resolution.

The time resolution of the system described above is mainly limited by the timing jitter between the two lasers, which is controlled by the synchronizing circuit. A higher resolution can be achieved by replacing the two lasers with an alternative set-up comprising one laser, a beamsplitter and a mechanical optical delay line, which is compatible with the novel delay-time modulation by pulse-picking. Although the measurable delay-time range with this set-up is typically limited to 1 ns, the time resolution is almost the same as the pulse width of the laser, which allows us to observe the carrier dynamics in a few-picosecond range (see 'Time Resolution' in Supplementary Information).

Received 2 April 2010; accepted 14 September 2010; published online 24 October 2010

References

1. Shinada, T., Okamoto, S., Kobayashi, T. & Ohdomari, I. Enhancing semiconductor device performance using ordered dopant arrays. *Nature* **437,** 1128–1131 (2005).
2. Shah, J. *Ultrafast Spectroscopy of Semiconductors and Semiconductor Nanostructures* (Springer, 1999).
3. Othonos, A. Probing ultrafast carrier and phonon dynamics in semiconductors. *J. Appl. Phys.* **83,** 1789–1830 (1998).
4. Binning, G., Rohrer, H., Gerber, Ch. & Weibel, E. Surface studies by scanning tunneling microscopy. *Phys. Rev. Lett.* **49,** 57–61 (1982).
5. Crommie, M. F., Lutz, C. P. & Eigler, D. M. Confinement of electrons to quantum corrals on a metal surface. *Science* **262,** 218–220 (1993).
6. Wiesendanger, R. (ed.) *Scanning Probe Microscopy and Spectroscopy: Methods and Applications* (Cambridge Univ. Press, 1994).
7. Heinrich, A. J., Lutz, C. P., Gupta, J. A. & Eigler, D. M. Molecule cascades. *Science* **298,** 1381–1387 (2002).
8. Lee, J. *et al.* Bandgap modulation of carbon nanotubes by encapsulated metallofullerenes. *Nature* **415,** 1005–1008 (2002).
9. Yoshida, S. *et al.* Microscopic basis for the mechanism of carrier dynamics in an operating p–n junction examined by using light-modulated scanning tunneling spectroscopy. *Phys. Rev. Lett.* **98,** 026802 (2007).
10. Hamers, R. J. & Cahill, D. G. Ultrafast time resolution in scanned probe microscopies. *Appl. Phys. Lett.* **57,** 2021–2033 (1990).
11. Nunes, G.Jr & Freeman, M. R. Picosecond resolution in scanning tunneling microscopy. *Science* **262,** 1029–1032 (1993).
12. Weiss, S., Ogletree, D. F., Botkin, D., Salmeron, M. & Chemla, D. S. Ultrafast scanning probe microscopy. *Appl. Phys. Lett.* **63,** 2567–2569 (1993).
13. Botkin, D. *et al.* Advances in ultrafast scanning tunneling microscopy. *Appl. Phys. Lett.* **69,** 1321–1323 (1996).

14. Groeneveld, R. H. M. & van Kempen, H. The capacitive origin of the picosecond electrical transients detected by a photoconductively gated scanning tunneling microscope. *Appl. Phys. Lett.* **69,** 2294–2296 (1996).
15. Pfeiffer, W. *et al.* Photoelectron emission in femtosecond laser assisted scanning tunneling microscopy. *Appl. Phys. B* **64,** 265–268 (1997).
16. Keil, U. D., Jensen, J. R. & Hvam, J. M. Transient measurements with an ultrafast scanning tunneling microscope. *Appl. Phys. Lett.* **72,** 1644–1646 (1998).
17. Khusnatdinov, N. N., Nagle, T. J. & Nunes, G Jr. Ultrafast scanning tunneling microscopy with 1 nm resolution. *Appl. Phys. Lett.* **77,** 4434–4436 (2000).
18. Grafström, S. Photoassisted scanning tunneling microscopy. *J. Appl. Phys.* **91,** 1717–1753 (2002).
19. Takeuchi, O. *et al.* Probing subpicosecond dynamics using pulsed laser combined scanning tunneling microscopy. *Appl. Phys. Lett.* **85,** 3268–3270 (2004).
20. Terada, Y. *et al.* Ultrafast photoinduced carrier dynamics in GaNAs probed using femtosecond time-resolved scanning tunneling microscopy. *Nanotechnology* **18,** 044028 (2007).
21. Kronik, L. & Shapira, Y. Surface photovoltage phenomena: theory, experiment and applications. *Surf. Sci. Rep.* **37,** 1–206 (1999).
22. Campbell, C. T. Ultrathin metal films and particles on oxide surfaces: structural, electronic and chemisorptive properties. *Surf. Sci. Rep.* **27,** 1–111 (1997).
23. Nilius, N., Wallis, T. & Ho, W. Development of one-dimensional band structure in artificial gold chains. *Science* **297,** 1853–1856 (2002).
24. Firt, P., Stroscio, J., Dragoset, R., Pierce, D. & Celotta, R. Metallicity and gap states in tunneling to Fe clusters on GaAs(100). *Phys. Rev. Lett.* **63,** 1416–1419 (1989).
25. Sze, S. M. *Physics of Semiconductor Devices* (John Wiley, 1981).
26. Schockley, W. & Read, W. T. Jr. Statics of the recombinations of holes and electrons. *Phys. Rev. Lett.* **87,** 835–842 (1952).

Acknowledgements

The authors thank Y. Hirayama of Tohoku University in Japan for stimulating discussions.

Author contributions

Y.T. performed the SPPX-STM experiment and data analysis. S.Y. assisted in the SPPX-STM experiment and laser operation. O.T. provided technical and theoretical advice. H.S. organized and supervised the project and edited the paper. All authors carried out extensive analysis of the results.

Additional information

The authors declare no competing financial interests. Supplementary information accompanies this paper at www.nature.com/naturephotonics. Reprints and permission information is available online at http://npg.nature.com/reprintsandpermissions/. Correspondence and requests for materials should be addressed to H.S.